

Gravity surface wave turbulence in a laboratory flume

Petr Denissenko¹, Sergei Lukaschuk¹ and Sergey Nazarenko²

¹ Fluid Dynamics Laboratory, the University of Hull, Hull, HU6 7RX, UK

² Mathematics Institute, The University of Warwick, Coventry, CV4-7AL, UK

February 9, 2020

Abstract

We present experimental results for water wave turbulence excited by piston-like programmed wavemakers in a water flume with horizontal dimensions $6 \times 12 \times 1.5$ meters. Our main finding is that for a wide range of excitation amplitudes the energy spectrum has a power-law scaling, $E_\omega \sim \omega^{-\nu}$. These scalings were achieved in up to one-decade wide frequency range, which is significantly wider than the range available in field observations and in numerical simulations. However, exponent ν appears to be non-universal. It depends on the wavefield intensity and ranges from about 6.5 for weak forcing to about 3.5 for large levels of wave excitations. We discuss our results in the context of the key theoretical predictions, such as Zakharov-Filonenko spectrum $\nu = -4$, Phillips spectrum $\nu = -5$, Kuznetsov's revision of Phillips spectrum (leading to $\nu = -4$) and Nazarenko's prediction $\nu = -6$ for weak turbulence in finite basins. We measured Probability Density Function of the surface elevation and good correspondence with the Tayfun shape except values near the maximum which we attribute to an anisotropy and inhomogeneity caused by the finite flume size. We argue that the wavenumber discreteness, due to the finite-size of the flume, prevents four-wave resonant interactions. Therefore, statistical evolution of the water surface in the laboratory is significantly different than in the open ocean conditions.

1 Introduction

Understanding statistical properties of the water surface waves is of great importance for a vast range of applications, from navigation and industrial activities at sea to modelling the transfer of momentum, heat, gases and aerosols through the air-sea interface. The latter are an important factor in improving weather and climate modelling and yet they are still very poorly understood. For example, a number of specialized centres and regional agencies provide a wave forecast for several days using certain assumptions about the wave statistics. Besides wave forcing by the wind, the other major ingredients of the models used by these

centres are the energy dissipation by wave breaking and the nonlinear interaction that takes place among waves with different length.

This nonlinear interaction is described by a theory called wave or weak turbulence theory (WT) introduced in the sixties by Zakharov and Hasselman (see [1] for history and details of WT). WT starts with the Euler equations for water with free surface in gravity field and derives a kinetic equation (KE) for the wave spectrum [2]. The central prediction of WT is a steady state energy spectrum obtained by Zakharov and Filonenko (ZF) [3],

$$E_\omega \propto \omega^{-\nu} \tag{1}$$

with the index $\nu = 4$. A number of hypotheses are needed in order to derive KE: weak nonlinearity, random phase approximation, homogeneity of the wave field. Conditions of validity of these hypotheses are still poorly understood. In addition, there exist an alternative approach originated by Phillips which assumed that the wave spectrum is not determined by weakly nonlinear dynamics but by strongly nonlinear sharp-crested waves which arise due to wavebreaking. This results in well-known Phillips power-law spectrum (PH) [4] with exponent $\nu = 5$. Perhaps even stronger uncertainty exists about the mechanisms and the form of wavebreaking arising in the random wave field.

Thus, there has been a significant effort to study the random waves and to test assumptions and predictions via field observations, laboratory experiments, numerical modelling. There are advantages and limitations in each of these approaches. The field observations of waves are done using buoys or ships [5] or remotely from aeroplanes [6]. They are extremely important because they measure the processes directly as they occur in nature. However, field observations are costly, have somewhat limited accuracy and lack of control over the observation conditions. This makes smaller-scale laboratory experiments and numerical modelling valuable parts of research.

Numerical experiments are naturally cheaper and controllable, but at present resolution they are not able to realise WT setup. Indeed, for the WT approach to be relevant it is essential that the nonlinear resonance broadening is greater than the spacing between the neighbouring wavenumbers, - otherwise most of the wave resonances are lost. As estimated in [7], this implies a condition on the minimal angle of the surface elevation

$$\gamma > 1/(kL)^{1/4}, \tag{2}$$

where L is the size of the basin. This is a very severe restriction meaning, e.g., that for a ten-kilometer wide gulf and meter-long waves one should have $\gamma > 0.1$.

Even for very small excitation amplitudes some resonances survive [8, 9, 10] and it is possible that they can support the energy cascade through scales even when condition (2) is not satisfied. Particularly, there have been numerous papers reporting results of the direct numerical simulations and claiming to confirm ZF spectrum, even though to satisfy condition (2) at a weakly nonlinear level $\gamma \sim 0.1$ one would have to compute at minimum 10000×10000 resolution which is much greater than the resolution of all previous simulations. Such a case, where the scalings and a qualitative behavior are the same as in an infinite system, and

yet there is a quantitative disagreement (e.g. in the energy cascade rate) was called in [9] “mesoscopic turbulence”.

On the other hand, due to necessity of numerical dissipation at high wavenumbers (to avoid the bottleneck effect) the inertial interval was very modest, - one decade in k i.e. less than half-decade in ω for gravity waves. This makes it very hard to judge about the exact value of the slope, particularly deciding between the ω^{-5} and the ω^{-4} spectra. Also, the water surface equations used in computations are truncated at the level of cubic nonlinearity and, therefore, become invalid for describing strongly nonlinear events, particularly the wavebreaking.

In this situation, performing laboratory experiments realising water wave turbulence looks especially attractive. Indeed, such experiments are significantly cheaper and controllable than the field observations and yet they are free from the artefacts of numerical modelling due to truncation and artificial dissipation, and they allow to resolve a significantly greater inertial range of scales.

The present paper describes the results of one of such experiments. Let us put our work in the context of the previous wavetank experiments aimed at studying nonlinear dynamics of random waves¹ Our work differs from the previous experiments in two respects. The wavetank is larger and has significant sizes in both horizontal directions that provides an opportunity to observe 2D wave evolution. We use a piston-type wavemaker rather than wind to produce waves. The wavemakers are more suitable for testing WT theory because they can force at low frequencies only while the wind forcing is spread over the wide frequency range. As a result, wavemakers enable to leave a more pure inertial range of scales for which ZF prediction was made. Larger size is important for minimising the finite-size effects and the k -space discreteness. Yet, as we will report in the present paper, the size of our tank is not large enough for WT theory to be applicable, and the wave field statistics was strongly affected by the finite-size effects.

2 Theoretical background

Below we describe the theoretical background and predictions that will serve us as reference points in interpretation of our experimental results. First of all, let us consider the predictions for the wave energy spectrum which is defined as,

$$E_\omega = \int e^{i\omega t'} \langle \eta(\mathbf{x}, t) \eta(\mathbf{x}, t + t') \rangle dt', \quad (3)$$

where $\eta(\mathbf{x}, t)$ is the surface elevation at time t and location in the horizontal plane \mathbf{x} . Here, the the integral is taken over a time window, and angle brackets mean ensemble averaging over realisations (a number of chosen time windows in the entire signal record). For statistically steady and homogeneous state, E_ω is independent of t and \mathbf{x} .

¹Here we are not concerned with the short-time experiments aimed at testing scaled models of sea installations or ships where the spectrum was pre-conditioned by wavemakers and the waves life time is not long enough for the nonlinearity to evolve.

2.1 Weak turbulence theory, ZF spectrum.

As we already mentioned in the introduction, WT theory considers weakly nonlinear random-phase waves in an infinite box limit. The central object of WT is KE for the wave spectrum, which in the context of water gravity waves called Hasselmann equation [2]. This equation is quite lengthy and for our purposes it suffices to say that ZF energy spectrum

$$E_\omega \propto \omega^{-4}$$

is an exact solution of Hasselmann equation which describes a steady state with energy cascading through an inertial range of scales from large scales where it is produced to the small scales where it is dissipated by wavebreaking.

It is crucially important that in deriving KE, the limit of an infinite box is taken before the limit of small nonlinearity. This means that in a however large but finite box, the wave intensity should be strong enough so that the nonlinear resonance broadening is much greater than the spacing of the k -grid (corresponding to Fourier modes in finite rectangular box). This is precisely the condition which, due to lack of available resolution, has never been satisfied in numerical experiments. As we will see below, this is also the reason why we never see the WT regime in our laboratory experiment.

2.2 Phillips spectrum and its relatives.

An easiest way to derive the PH spectrum is to assume that the gravity constant g is the only relevant dimensional physical quantity. Then the wave energy spectrum is uniquely determined in terms of g and ω based on the dimensional analysis [4],

$$E_\omega = g^2 \omega^{-5}. \quad (4)$$

It is quite clear that this argument is equivalent to saying that the linear term is of the same order as the nonlinear one in the water surface equations in Fourier space. Such a balance of linear dispersion and nonlinear terms is typical for soliton-like nonlinear structures.

Physically, the PH spectrum is usually associated with the sharp crested waves, so that the short-wave Fourier asymptotics are dominated by discontinuous slopes of such wavecrests. Assuming first, that such a discontinuity is happening at an isolated point (i.e. in a cone-like structure) we get for the one-dimensional energy spectrum in wavenumber space

$$E_k \propto k^{-3}. \quad (5)$$

Second, assuming that transition from the k -space to the ω -space should be done according to the linear wave relation $\omega = \sqrt{gk}$, we arrive at the PH spectrum (4).

Kuznetsov [11] questioned both of these assumptions and argued that (i) slope break occurs on one-dimensional lines/ridges rather than zero-dimensional point/peaks, and (ii) that the wave-crest is propagating with preserved shape, i.e. $\omega \propto k$ should be used instead of the linear wave relation $\omega = \sqrt{gk}$. This assumptions give $E_\omega \propto \omega^{-4}$, i.e. formally the same scaling as ZF, even though the physics behind it is completely different.

Finally, it was proposed in [12] that wavecrest ridges may have non-integer fractal dimension somewhere in the range $0 < D < 2$. Assuming, following Kuznetsov, $\omega \propto k$, we have in this case

$$E_\omega \propto \omega^{D-6}. \quad (6)$$

In our experimental results reported below, at large forcing levels we observe the prominent wavebreaking events the role of which in forming spectra is quite apparent. However, the spectrum exponent appears to be dependent on the forcing intensity. Possibly this could be due to dependence of wavebreaking morphology and dimension D on the wave turbulence intensity.

2.3 Discrete wave turbulence.

Here, we will briefly describe the theory suggested in [7] for the case of very weak turbulence in discrete k -space. As we already mentioned, for the WT mechanisms to work, the four-wave resonances must be broad enough to cover simultaneously many discrete k -modes, and this condition in terms of the surface slope γ gives the estimate (2). What happens if the waves are so weak that this condition is not satisfied? In this case, the number of exact and quasi four-wave resonances will be drastically depleted [13, 14, 7]. This will lead to the arrest of the energy cascade from long to short waves and, therefore, there will be an accumulation of the spectrum near the forcing scale. Such an accumulation will proceed until the intensity is strong enough for the nonlinear broadening to become comparable to the k -lattice spacing, i.e. when condition (2) will become marginally satisfied. At this point, the four-wave resonances will get engaged and the spectrum “sandpile” will tip over toward the higher wavenumbers. This process will proceed until the whole k -space will be filled by the spectrum having a critical slope determined by the condition that the wave-resonance broadening is of the order of the k -grid spacing for all modes in the inertial range. This condition gives the following spectrum

$$E_\omega \propto \omega^{-6}.$$

2.4 Probability density functions.

Some important information about the wave field statistics, not contained in the spectra, can be accessed by measuring the probability density function (PDF) of the surface elevation. We remind for reference that homogeneous isotropic wave fields with random independent phases of all of its modes are characterized by Gaussian PDF shape. The Gaussian shape is expected for linear and weakly nonlinear waves, provided the conditions of homogeneity and isotropy are satisfied. The PDF for stronger nonlinearities was obtained by Tayfun [15] using a model where the wave field is made of independent weakly nonlinear Stokes waves whose first harmonics are gaussian. Tayfun distributions were found to be in good agreement with numerical simulations with wide-angle quasi-isotropic wavefields [16] and to much lesser extent in narrow-angle distributions [17, 18].

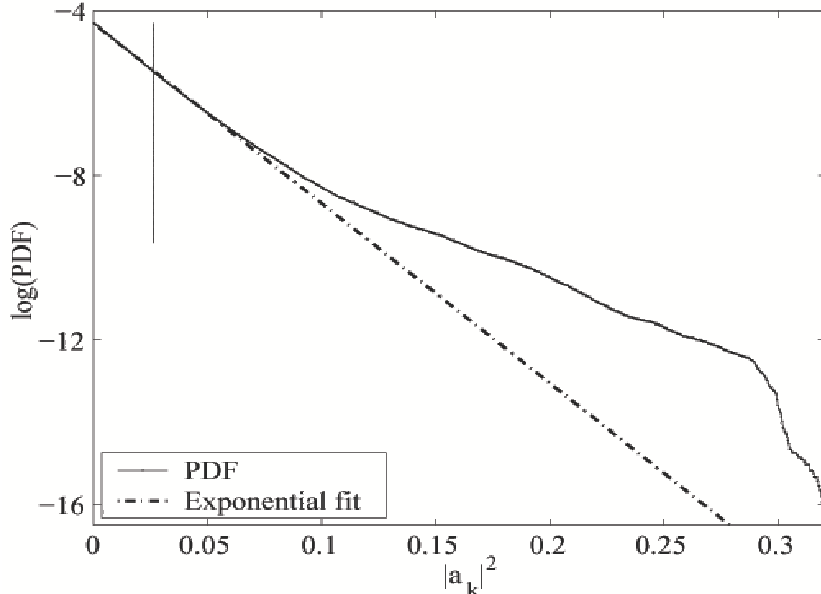


Figure 1: Numerically obtained PDF of spectral intensity in a small band around ω equal to the eight minimal wave frequencies [8, 10].

Another interesting statistical object is a PDF of the spectral intensities (squared modules of the Fourier coefficients) at a particular fixed frequency ω . Based on a generalized WT approach, it was found theoretically in [8] that such a PDF may differ from the Rayleigh distribution (corresponding to Gaussian wave fields) by significantly fatter tails. This corresponds to a probability to observe strong waves more frequently than for Gaussian waves (a “freak wave” effect).

A typical form of such a PDF obtained in numerical experiments [8, 10] by applying band-pass filtering with $\Delta\omega \ll \omega$ is shown in Figure 1. Indeed, we see a significant deviation in the tail from Rayleigh shape (straight line in Figure 1). Later in the present paper we will observe a similar effect in our experimental results.

3 Experimental setup

Our experiments with surface gravity waves were conducted in a rectangular tank with dimensions 12 x 6 x 1.5 meters filled with water up to the depth of 0.8 meters. The wavemaker consists of 8 vertical paddles of width 0.75 m covering the full span of one short side of the tank, see Figure 2. Each paddle can oscillate horizontally in the direction perpendicular to its face plane. Amplitude, frequency and phase can be set for each panel independently allowing, in principle, to control directional distribution of the generated waves. A motion controller is used to program parameters of the generated wavefield by specifying amplitude, frequency distribution and a number of wavevector directions.

In all experiments described in the present paper, the frequency bandwidth generated

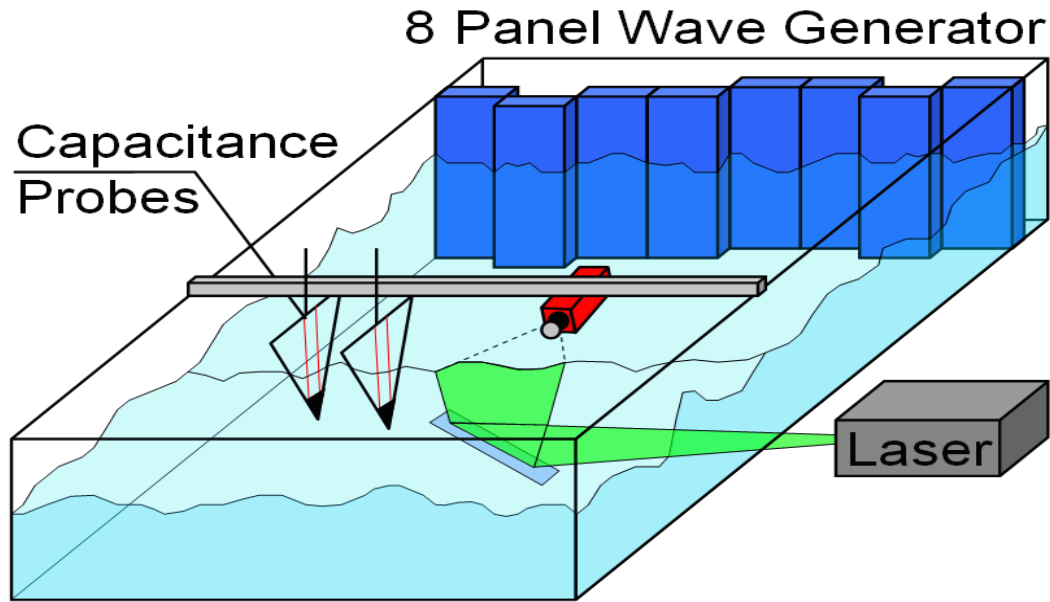


Figure 2: Experimental setup at “The Deep” flume.

by the wavemaker had a fixed broadband distribution in the range 0.4 to 1.2 Hz, which corresponds to the wavelengths 1 to 3.9 m. To get more spatially isotropic excitations, the wavevector directions were chosen within a 90-degree sector enabling the multiple reflections (10^4) even for the shortest excited wavelengths (an attenuation length for one meter waves on deep water is about 10^4 m [19]). The main control parameter was an excitation amplitude on the wavemaker, and we performed the experiments at different values of this parameter to study dependence of the spectrum and PDFs on the average wave turbulence intensity. The surface elevation was measured simultaneously by two capacitance gauges, A and B, positioned in the middle part of the tank. A-gauge was fixed while another could move parallel to the short flume side, so that the distance between the gauges could vary from 0.1 to 2.5 m, see Figure 2. In most of the reported experiments this distance was 40 cm. Each probe consists of two parallel vertical wires separated by 1 cm distance. Due to the difference in the dielectric permeability of water and air, the coupling capacitance between the wires depends on their submergence depth. This capacitance was measured using sinusoidal AC with different frequencies used for each gauge (60 and 90 kHz) to avoid a crosstalk between them. Signals from the gauges were amplified by two lock-in amplifiers. The outputs from the amplifiers were digitised by a multi-functional board (NI6035, National Instruments) and stored as a waveform using LabView software. Typical parameters of the acquired signals were as follows. The bandwidth at the lock-in amplifier output was 32 Hz, the sampling rate was 400 Hz for each channel, the minimum acquisition time was 2000 seconds. The gauges were calibrated before the measurements in the same tank with a stationary water surface. The experimental data set contains a number of two-channel waveforms acquired at different amplitudes of the generated waves and for two different configurations of the wavemaker paddles. In one configuration all eight paddles were used, in others only seven or

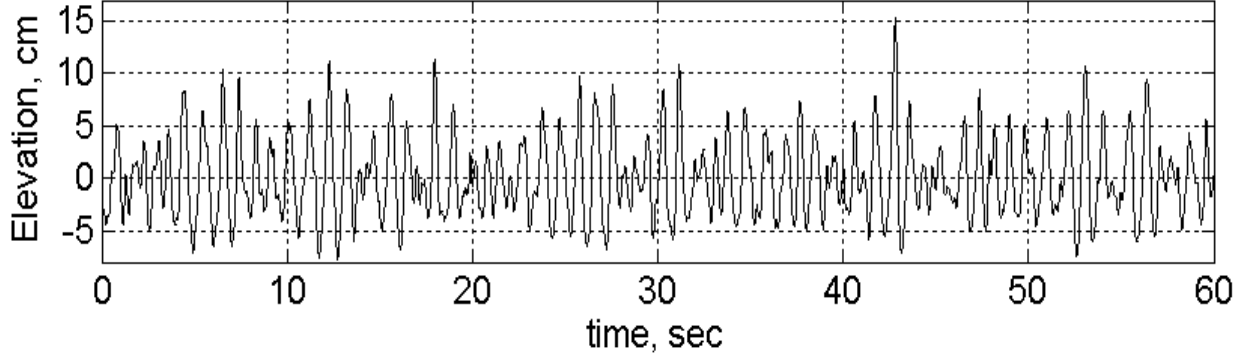


Figure 3: Typical signal for the time evolution of the surface height at one of the gauges.

six paddles worked while one or two corner paddles were disconnected. Although using the six and seven paddle configurations were caused by technical reasons, these additional data enable us to compare results with different wave excitation geometries. The measurement procedure was the same during the whole experiment and consisted of setting the excitation wave amplitude, waiting for 15 minutes of transient time, measuring and writing the signals during the next 30-60 minutes. A typical time signal, the wave elevation vs time, is shown in Figure 3

Collected waveforms were processed using Matlab. The common initial part for all data processing procedures included high-pass filtering with the time constant 0.01 s eliminating a slow drift of signals, decimation to the sampling frequency 50 Hz, and elimination of the initial transitional part of signals. At the next stage of processing we evaluated the statistical characteristics of waves: the spectra (by applying the fast Fourier transform), the PDF of the surface height and the PDF of Fourier modes (by band-pass filtering).

One of the quantities we have used to characterize the wave field strength was the RMS of the wave height,

$$A = \sqrt{\langle (\eta - \eta_0)^2 \rangle}, \quad (7)$$

where $\eta = \eta(t)$ is the water surface elevation at the gauge position and η_0 is its mean value. Here, the angle brackets denote the time averaging over the whole measuring interval. As a characteristics of nonlinearity, we used the mean slope at the energy containing scale,

$$\gamma = k_m A, \quad (8)$$

where k_m is the wavenumber corresponding the the maximum of the energy spectrum. In all our experiments k_m was approximately the same and located in the forcing range, $k_m \approx 5.7\text{m}^{-1}$ which corresponds to the wavelength $\lambda \approx 1.1$ m. Note that in the same experiment waves with different frequencies usually have different nonlinearities. Depending on the spectrum slope ν , the nonlinearity may be smaller at higher frequencies (for $\nu > 5$) or greater (for $\nu < 5$). One can see that PH spectrum is a borderline case in which the nonlinearity is the same at all frequencies.

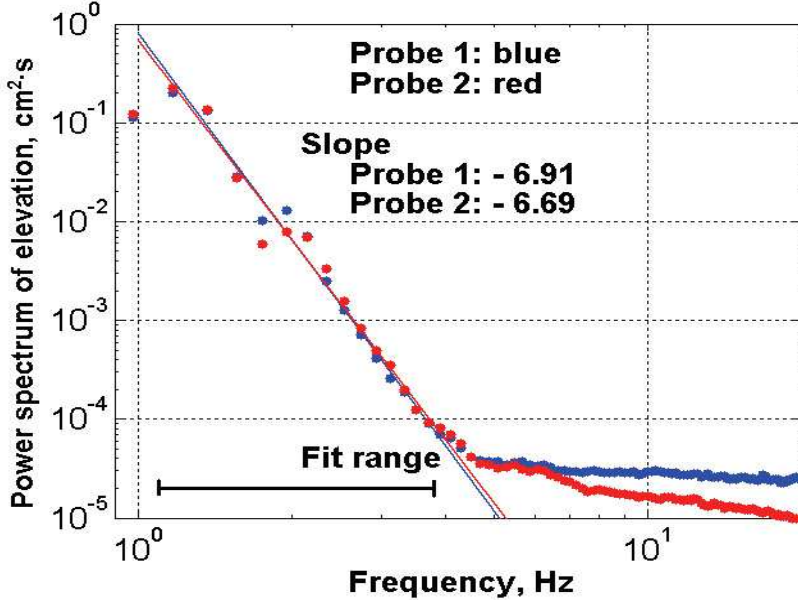


Figure 4: Spectrum obtained in an 6-paddle experiment with low intensity, $A \approx 1.9$ cm ($\gamma \approx 0.11$).

In our experiments we covered the range of excitations from very weak waves with mostly smooth surface and occasional seldom wavebreaking, $A \approx 1.3$ cm and $\gamma \approx 0.075$, to very strong wave amplitudes characterized by a choppy surface with numerous wavebraking events, $A \approx 5.2$ cm and $\gamma \approx 0.30$.

3.1 Spectra

To find spectra we used the Welch algorithm with the Hanning window of length 4096 points (10.24 s) and the averaging performed over about 700 spectral estimates for each signal record. Typical results for the spectra for several different levels of nonlinearity is shown in Figures 4, 5 and 6.

Horizontal lines show an interval where the spectrum slope (index) is estimated using linear least-square logarithmic fit. The maxima of spectra in all cases are at about 1.2 Hz which corresponds to the highest frequency in the pumping wave. Lower frequencies have less power relative to the spectrum maximum due to the dumping of long waves by the bottom friction. One can see that the scaling behavior is not-so-well formed in Figure 4 which corresponds to the weakest wave field intensity $A \approx 1.85$ cm and $\gamma \approx 0.11$, and this leads to some uncertainty in the value of the slope and its sensitivity to the choice of the fitting range. On the other hand, the spectra corresponding to the medium and the strongest intensities, shown in Figures 5 and 6 respectively, exhibit clear scaling ranges which are up to one decade wide and have well-defined slopes. The results for the slopes obtained in different experiments, including the cases with six and seven working paddles, are summarized in Figure 7 with the slope uncertainty indicated by the vertical bars. The

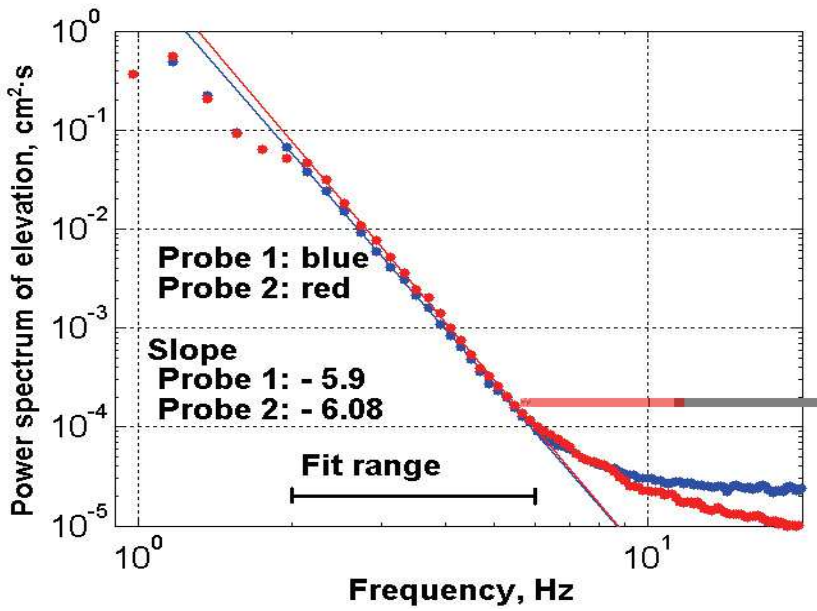


Figure 5: Spectrum obtained in an 6-paddle experiment with medium intensity, $A \approx 3.05$ cm ($\gamma \approx 0.17$).

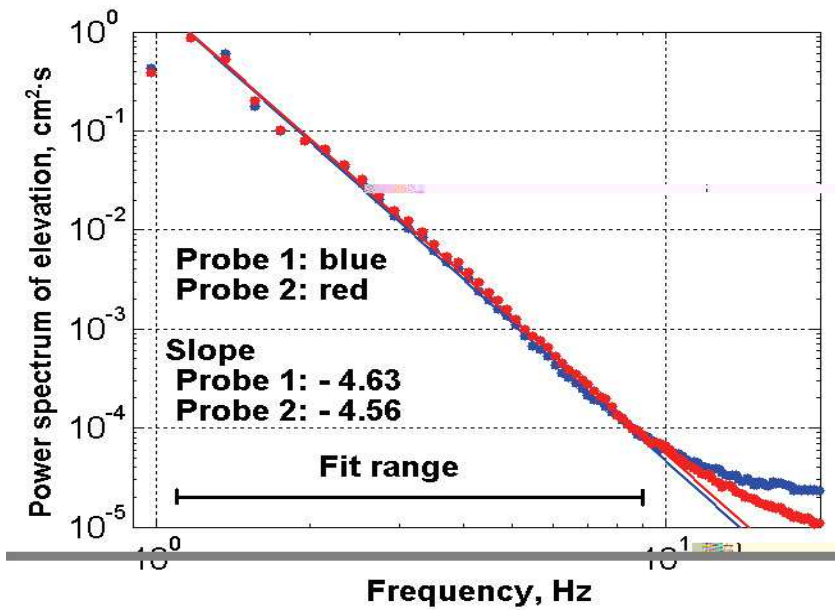


Figure 6: Spectrum obtained in an 7-paddle experiment with high intensity, $A \approx 3.73$ cm ($\gamma \approx 0.21$).

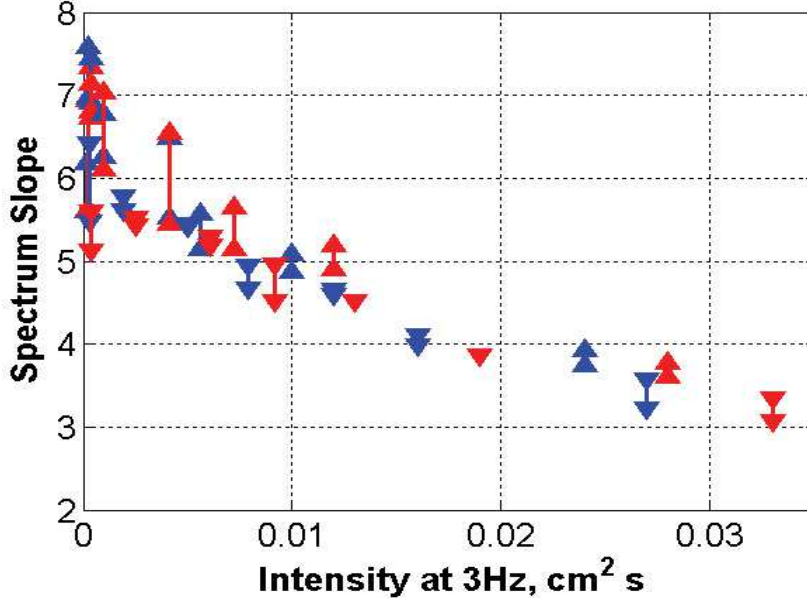


Figure 7: Plot of observed spectral slopes in the 6-paddle and 7-paddle experiments versus the spectrum intensity at 3 Hz.

bars were constructed by varying the fitting range and finding the minimal and the maximal slopes. The x -axis represents the intensity value of the spectrum at 3Hz frequency, E_{3Hz} . The reason for this choice of measure of the wave turbulence intensity is that this quantity appears to be more universal than the RMS of the surface elevation, A , or RMS of the slope parameter γ . This is because the latter two are dominated by the energy containing scale which appears to be different for the 6-paddle and the 7-paddle series of experiments. On the other hand, 3 Hz is within the scaling (equilibrium) range of all spectrum data sets, and the data points for the slope values ν for the six- and seven-paddle experiments collapse much better on the same curve if E_{3Hz} is used as a measure of intensity.

The general trend, clear in Figure 7, is that the slope ν is much steeper for the weak wave fields with respect to the strong ones. One can see that at small amplitudes the data scatter and uncertainty are much greater at low intensities than for stronger wave turbulence. For experiments with the minimal intensity, $A \approx 1.85$ cm and $\gamma \approx 0.11$, we have $\nu \approx 6.3 \pm 1.2$, which is in good qualitative agreement with the prediction $\nu = 6$ made in [7] for the critical spectrum where the nonlinear resonance broadening is of the same magnitude as the mean spacing between the discrete k -modes. Thus, we indirectly confirm that the k -space discreteness (caused by the finite flume size) plays a defining role in shaping the frequency spectrum at low wave excitations. We see that the condition (2) is not quite satisfied,

$$\gamma \approx 0.11 < 1/(k_m L)^{1/4} \approx 0.36.$$

Note that (2) is only an order of magnitude estimate so factor 3.3 discrepancy could easily be an order one coefficient (like π) unaccounted by (2). On the other hand, it might also

mean that an efficient energy cascade may start even at the level or resonance broadening which remains less than the k -grid spacing. In this case not all of the four-wave resonances are equally engaged, and that most of the energy cascades from low to high wavenumbers are carried by most active quartets of modes which causes extra anisotropy of wave turbulence. Such an anisotropy could also be a natural reason for deviations from the pure power-law scaling seen as a significant slope uncertainty and scatter at low intensities in Figure 7.

At large wave field intensities, one can see in Figure 7 a much better scaling behavior with significantly smaller scatter or uncertainty in the slope values. There is a range of intensities where the PH slope $\nu = 5$ is observed, and we report that wave breaking events were common for such intensities. At higher intensities, one can see the $\nu = 4$ slope which is predicted by both ZF and Kuznetsov theories [3, 11]. However, the water surface was visibly very choppy with numerous frequent wavebreaking and high values of the surface slope, $\gamma > 0.2$, and rules out the weak nonlinearity assumption which is the basis of ZF theory [3]. Kuznetsov theory [11] is more likely to be relevant to these conditions, because it derives $\nu = 4$ value from considering strongly nonlinear wavecrests with sharp 1D ridges and the speed of which is nearly constant while they pass the height gauge. However, there is no visible plateau in Figure 7 at $\nu = 4$ value and ν takes bigger values at lower intensities and lower values for greater amplitudes (reaching $\nu = 3.3$ for the maximum intensity of $\gamma \approx 0.3$). As we mentioned before, such a change of slope could be explained by changing the fractal dimension of the wavecrest ridges, from $D = 0$ cone-like splashes giving $\nu = 5$ at smaller amplitudes (PH case), set of 1D lines giving $\nu = 4$ at larger amplitudes (Kuznetsov) to more complex fractal curves at the highest intensities with $1 < D < 2$ giving $3 < \nu < 4$. Note that [12] obtained value $D = 3/2$ by considering scalings of the higher moments within the wave turbulence formalism.

3.2 Probability density functions.

Our results for PDF of the surface elevation measured for different wave intensity levels, for different numbers of working paddles (6 or 7) and for different locations (at gauges A and B) are shown in Figures 8, 9 and 10. One can see good qualitative agreement of PDFs with the Tayfun distribution at all intensities, - low at Figure 8, medium at Figure 9 and high at Figure 10. However, one can notice rather irregular deviations, especially near the PDF maximum corresponding to probability of waves with less-than-mean intensities. We have checked that these deviations are real and are not fluctuations due to insufficient statistical data. To do this, we split a long record corresponding to one of experiments into two shorter sub-sets, and we observed that the resulting PDFs for both sub-sets were identical to the PDF obtained from the original long record. One can also see that the observed deviations from Tayfun were different at the same experiment for two different locations (i.e. at gauges A and B).

Now let us consider PDFs of the spectral intensities obtained by band-pass filtering of the time signal with a narrow pass window $\Delta\omega$ around a particular frequency ω ($\Delta\omega \ll \omega$). These PDFs for the experiments with low and high mean intensities of the wave field are shown in Figures 11 and 12 correspondingly. One can see a similar picture as in numerical

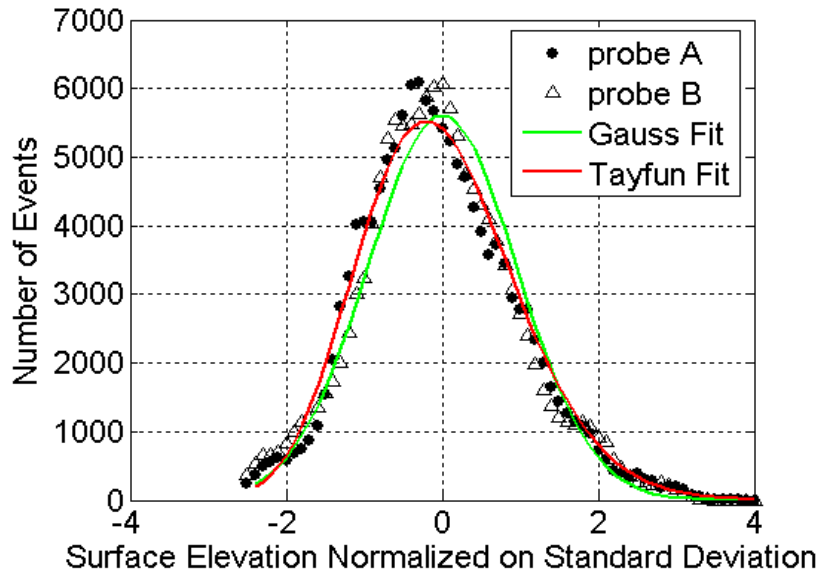


Figure 8: PDF of the surface height at locations of gauges A (dots) and B (triangles) in the 6-paddle experiment for mean intensity $A = 1.85\text{cm}$ ($\gamma = 0.11$).

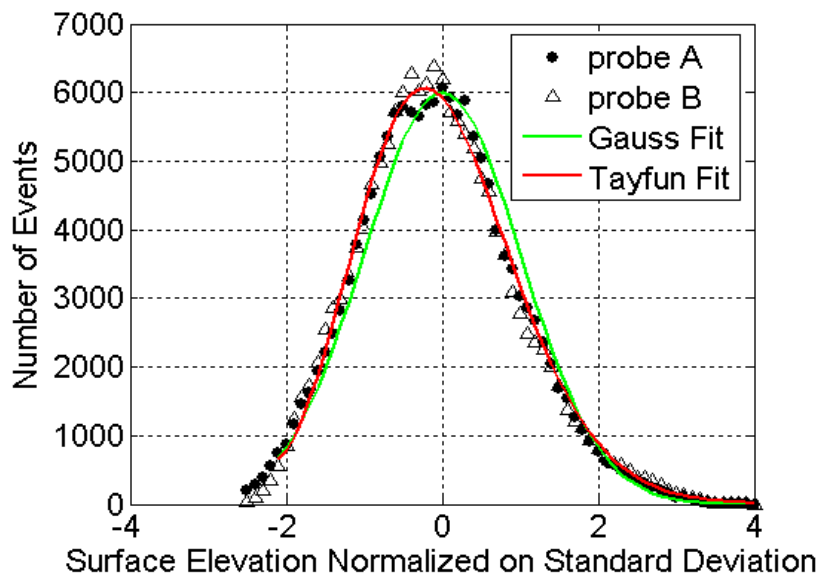


Figure 9: PDF of the surface height at locations of gauges A (dots) and B (triangles) in the 6-paddle experiment for mean intensity $A = 3.05\text{cm}$ ($\gamma = 0.17$).

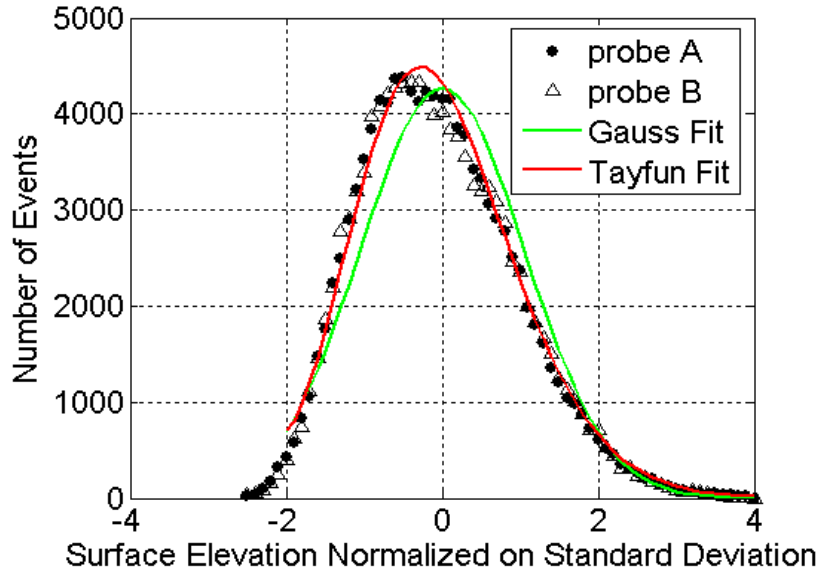


Figure 10: PDF of the surface height at locations of gauges A (dots) and B (triangles) in the 7-paddle experiment for mean intensity $A = 3.73\text{cm}$ ($\gamma = 0.213$).

results shown in Figure 1, namely much higher with respect to the Rayleigh distribution probability of strong waves. This is a nonlinear effect and, therefore, it is natural that it is more pronounced for higher intensities (i.e. in Figure 12).

4 Conclusions

One of the main observations derived from our experimental results is that the slope of the wave spectrum is not universal: it takes high values, around 6.5, for weak wave fields and gradually decreases as one increases the wave field intensity to the value of about 3.5 when the wave field is very choppy with a lot of wavebreaking. In the absence of forcing, one would expect KAM-like behavior for most of the k -space because only a tiny fraction of modes on the discrete k -lattice can satisfy the exact four-wave resonant conditions [13, 14, 7]. However, our system had a continuous forcing and the spectrum can grow until it reaches a critical slope where the nonlinear resonance broadening becomes comparable to the k -grid spacing, and the spectrum “sandpile” can “tip over” producing intermittent avalanches carrying energy from large to small scales. Such a critical spectrum was argued in [7] to have slope 6, which is in a good qualitative agreement with our observations. For larger amplitudes, we see a gradual decrease of the slope, possibly due to the sharp wavecrests whose fractal dimension decreases with increasing wave intensity (from $D = 0$ for PH spectrum, to $D = 1$ for Kuznetsov spectrum, to $1 < D < 2$ for the strongest and most choppy wave fields. We emphasize that at this point dependence of D in the wave intensity is purely speculative, and a careful study of the wavebreaking morphology is needed to be done to measure D in

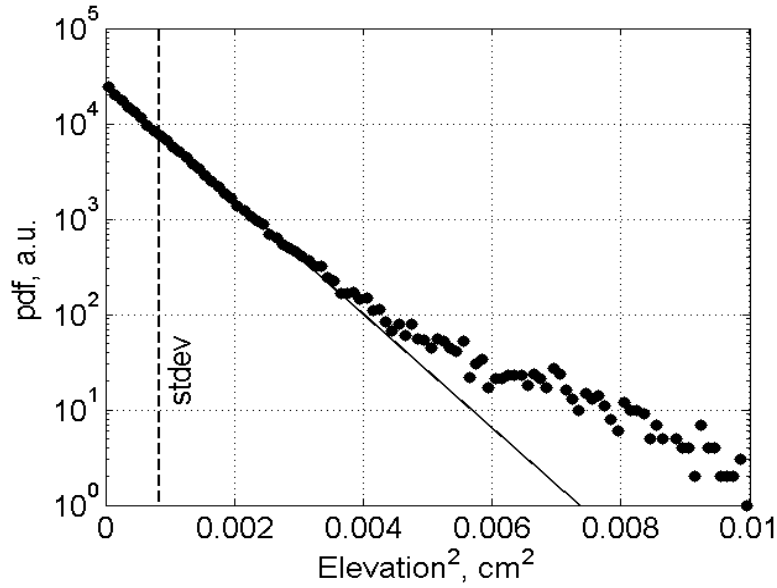


Figure 11: PDF of the surface elevation signal band-pass filtered with frequency window $\Delta f = 1Hz$ centered at $f = 6Hz$. The signal corresponds to probe B in a low-intensity experiment with mean elevation $A = 1.85cm$ ($\gamma = 0.11$)

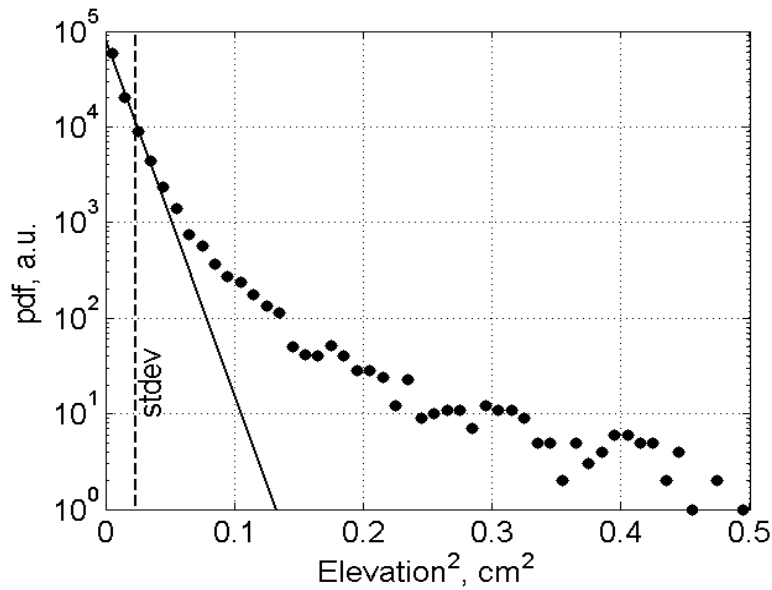


Figure 12: PDF of the surface elevation signal band-pass filtered with frequency window $\Delta f = 1Hz$ centered at $\omega = 6Hz$. The signal corresponds to probe B in a high-intensity experiment with mean elevation $A = 3.73cm$ ($\gamma = 0.213$)

experiments.

Another aspect of our study was the measurement of PDFs of the wave elevations which, as expected, agree well with the Tayfun distribution even though the flume finite-size effects are indeed seen to lead in irregular deviations from the perfect Tayfun shape. We also observed higher than in Gaussian fields probability of strong wave modes in the way similar to theoretical predictions and numerical simulations of [8, 10].

The major feature of our experiments was that the WT regime was never achieved: with increasing wave intensity the nonlinearity becomes strong before the system loses sensitivity to the k -space discreteness. Particularly, most of the four-wave resonances remained arrested leading to a depletion of the energy cascade from low to high wavenumbers. Thus, being interesting in their own way, laboratory waves undergo a significantly different statistical evolution from the one of their open-sea counterpart. In our future work we will explore possibilities to “confuse” the laboratory flume and make it “forget” about the finite-size effects via breaking the regular k -space structure by distorting the perfect-rectangle shape of the flume boundaries. The goal of such exercise would be to increase realism of laboratory modeling of the ocean surface processes.

References

- [1] V.E. Zakharov, V.S. L’vov and G.Falkovich, ”Kolmogorov Spectra of Turbulence”, Springer-Verlag, 1992;
- [2] K. Hasselmann, J. Fluid Mech. **12**, 481 (1962);
- [3] V.E.Zakharov and N.N. Filonenko, J. Appl. Mech. Tech. Phys. **4** , 506-515 (1967);
- [4] O.M. Phillips, The equilibrium range in the spectrum of wind generated waves. J. Fluid Mech. **4**, 426-434, 1958;
- [5] W. J. Pierson and L. Moskowitz, A proposed spectral form for fully developed wind seas based on the similarity theory of S. A. Kitaigorodskii. J. Geophys. Res., **69**, No. 24, 5181-5190 (1964);
- [6] C. Elachi, Physics and Techniques of remote sensing, John Wiley & Sons Pu., New York, USA, 1987.
- [7] S.V. Nazarenko, Sandpile behaviour in discrete water-wave turbulence, J. Stat. Mech. L02002 (2006) doi:10.1088/1742-5468/2006/02/L02002 (arXiv:nlin.CD/0510054).
- [8] Y. Choi, Y. Lvov, S.Nazarenko and B.Pokorni, Anomalous probability of large amplitudes in wave turbulence, Physics Letters A, **339**, Issue 3-5, 361-369 (2005); (arXiv:math-ph/0404022 v1 Apr 2004).
- [9] V. E. Zakharov, A. O. Korotkevich, A. N. Pushkarev and A. I. Dyachenko, Mesoscopic wave turbulence, JETP Letters, **82**, Number 8, October, 487 (2005);

- [10] Y. Lvov, S.Nazarenko and B.Pokorni, Discreteness and its effect on water-wave turbulence , *Physica D* , **218**, Issue 1, 24-35 (2006); (arXiv: math-ph/0507054 v1 July 2005).
- [11] E.A. Kuznetsov, Turbulence spectra generated by singularities, *JETP Letters*, **80**, 83-89, (2004);
- [12] C.Connaughton, S.Nazarenko, A.C.Newell, *Dimensional analysis and weak turbulence*, *Physica D*, **184**, 86-97 (2003);
- [13] E.A. Kartashova, On properties of weakly nonlinear wave interactions in resonators, *Physica D* **54**, 125 (1991).
- [14] E.Kartashova, *Wave resonances in systems with discrete spectra*, *AMS Transl. (2)* **182** (1998);
- [15] M.A.Tayfun, Narrow-band nonlinear sea waves. *J. Geophys. Res.* **85**, 1548-1552, (1980);
- [16] Socquet-Juglard, K.B. Dysthe, K. Trulsen, H.E. Krogstad, and J. Liu, Probability distributions of surface gravity waves during spectral changes. *J. Fluid Mech.* **542** 195-216 (2005);
- [17] Onorato, M., Osborne, A.R., Serio, Cavaleri, L., Brandini, C., and Stansberg, C.T., Observation of strongly non-Gaussian statistics for random sea surface gravity waves in wave flume experiments *Phys. Rev E* **70** (6): Art. No. 067302 (2004);
- [18] M.Onorato, A.R. Osborne, M.Serio, On Deviations from Gaussian Statistics for Surface Gravity Waves. arXiv:nlin.CD/0503071, v1 (2005);
- [19] J. Lighthill. *Waves in Fluids*. Cambridge University Press, 2005. p 235.